Influence of GO concentration on photoconversion efficiency for dye-sensitized solar cells using GO:TiO₂-AD as photoanodes

M. J. AlSultani, M. F. A. Alias

University of Baghdad, College of Science, Physics Department, Baghdad, Iraq
[*]) Email: may20131313@yahoo.com

Spray pyrolysis is used to make GO:TiO₂ hybrid photoanodes immersed in anthocyanin dye extracted from red cabbage using various GO concentrations for dye-sensitized solar cells (DSSC). The effects of GO and anthocyanin dye on structural, morphological, optical, and electrical properties are examined. X-ray diffraction showed GO:TiO₂-AD hybrid photoanodes have an anatase phase. Increased GO concentration leads to a reduced crystallite size from 19.84 to 15.04 nm. Field emission scanning electron microscope (FESEM) and atomic force microscope (AFM) are used to examine photoanodes morphology, grain size, and surface roughness. Due to the GO's 2D structure, adding it to hybrid photoanodes created a continuous TiO₂ network. This incorporation reduced grain size from 60.9 to 52.8 nm, increasing surface area and roughness from 16.8 to 41.7 nm. These changes improved photoanodes' dye absorption, light harvesting, and photocurrent density (J). Hall-effect measurements at room temperature showed a significant increase in conductivity and carrier concentration of about one and three orders of magnitude, respectively. The results have indicated that the best GO concentration is 4%. The J-V characterization, short circuit current density, J_{SC}, open circuit voltage, V_{OC}, filling factor, F.F., and PCE of the prepared DSSC have 28.85 mA/cm², 0.52 V, 53.79%, and 6.14% values, respectively. The synthesized GO:TiO₂-AD photoanodes are high-quality and suitable for energy conversion devices.

Keywords: GO:TiO₂; Anthocyanin Dye; Hybrid Photoanodes; J-V Characterization.

1. INTRODUCTION

The most potential renewable energy sources for maintaining the current energy supply in this environment is solar energy [1,2]. As part of a photoelectrochemical system, dye-sensitized solar cells (DSSCs) are the most efficient third-generation solar technology available today [3]. The first dye-sensitized solar cell is built and displayed by Grätzel and O'regan in 1991. It consisted of a visible light absorber, a wide band gap nanocrystalline n-type semiconductor, fluorine-doped tin oxide glass (FTO), a redox couple electrolyte, and a platinum counter electrode [4]. Changes in electrode composition, dye molecular engineering, electrolyte choice, and substrate use can all improve DSSC performance. Although DSSCs are not the most efficient thin film cells, their transparency, low cost, wide range of light absorption, suitability for flexible substrates, and possibility for large scale manufacturing make them useful for research. In DSSC, the photoanode material plays a critical role in dye loading, electron injection, transportation, and collection, all of which affect photoconversion efficiency. The selection is based on having a high surface area for enhanced dye adsorption and matching the energy gap of the semiconductor with that of the dye. Numerous photoanode materials, including metal/metal oxide-TiO_2 hybrids, doped TiO_2, porous TiO_2 structures, composite and core-shell structures [5–9], and TiO_2 - carbon materials, have been developed in an effort to improve electron transport and decrease recombination [10–12]. Currently, the most effective photoanode for DSSCs is nanocrystalline TiO_2 film because to its unique photoelectronic and photochemical features, such as its high chemical stability, optimum C.B edge position, and environmental friendliness [13]. Because of its broadband gap, suitable band edge levels for charge injection and extraction, longer lifetime of excited electrons, strong resistance to photo corrosion, nontoxicity, and affordability, titanium dioxide (TiO_2) is frequently employed in solar energy applications [14]. Unoccupied Ti^{+4} 3d bands make up the bottom of the conduction band, and filled O^{-2} 2p bands make up the top of the valence band. Shallow electron traps are produced by oxygen vacancies, titanium interstitials, and modified crystal surfaces, which can increase TiO_2 conductivity doping is a useful technique to purposefully introduce impurities into the lattice structure of TiO_2 to modify its electrical properties. The atomic radius of the dopant should closely match that of the ion it replaces to prevent lattice deformation and the development of new defects that could impair device performance. Improved dye molecule binding to semiconductor material nanostructures boosts photon absorption and electrical energy conversion. Anthocyanin pigment has been used as the dye sensitizer in DSSC in several experiments [15,16]. A naturally occurring pigment called anthocyanin gives plants, fruits, flowers, and leaves their color. It absorbs light between 450 and 600 nm in wavelength and appears purple red most of the time. The anthocyanin pigment's carbonyl and hydroxyl group chains act as anchoring agents, allowing the pigment to attach to TiO_2 nanostructures. An important determinant of the DSSC's energy conversion efficiency is this interaction [17]. Due to its remarkable electrical conduction in two dimensions and zero band gap, graphene, a 2D carbon nanomaterial, has attracted a lot of attention. In this case, GO is used to form a GO:TiO_2 Schottky junction that prevents recombination. The formation of bridges enabled electron transport through the TiO_2 network, while π-π interactions led to dye adsorption, both of which improved the photoelectrical conversion efficiency [18]. Using charge transfer interaction, electrostatic binding, or physisorption, TiO_2 nanoparticles are firmly affixed to the GO flakes. As a very effective electrical conductor, graphene oxide (GO) enhances electron transit from TiO_2 conduction band, hence decreasing recombination [19]. In this study, GO:TiO_2 anthocyanin dye photoanodes are fabricated using the chemical spray pyrolysis method. This photoanodes are an exciting choice for uses in DSSCs.

2. EXPERIMENTAL PART
2.1 Materials Details

The process involved depositing GO:TiO$_2$ films onto FTO substrates using spray pyrolysis and then immersing them in anthocyanin dye for 24 h. The Hummer method created graphene oxide by combining 10 g of graphite powder, 4 g of NaNO$_3$, 6 g of KMnO$_4$, and 0.01 g of boric acid with 100 ml of concentrated H$_2$SO$_4$ in an ice bath at 0–5 °C for 1 h. Slowly include 5 g of KMnO$_4$, and the mixture is stirred at 35°C for 2h, then 250 ml of distilled water and 12 ml of hydrogen peroxide are added and stirred at 95°C for 30 min. The suspension is centrifuged, rinsed, and filtered. The graphene oxide is desiccated at 40°C for 24 h. Amounts of powder of graphene oxide (0.05, 0.1, 0.2, 0.3, 0.4, and 0.5 g) are dissolved in 10 ml of acidified ethanol solvent, resulting in concentrations of 0.5, 1, 2, 3, 4, and 5%, respectively. The precursor suspension is prepared by combining titanium tetra isopropoxide (TTIP from Sigma-Aldrich), glacial acetic acid, deionized water, and concentrated nitric acid. The solution is agitated for 30 min until clarity is achieved. The suspension is re-condensed at 80°C for 90 min. 0.4 g of titanium (IV) nanopowder (Anatase from Skyspring Nanomaterials, Inc.) is added to 10 ml of precursor liquid in the suspension, followed by 250 µl of deionized water and 12 ml of acidic ethanol. The solution underwent 480 s of sonication after 15 min of agitation. The process involves chopping 50 g of red cabbage leaves with a mixture of methanol, acetone, and distilled water according to the proportions (2:1:1). The mixture is then placed in a water bath at 50°C for an hour. After that, 3 drops of HCl are added to the dye extract, and the solution is filtered. The filtered solution is placed in a rotary evaporator to remove the ethanol, acetone, and distilled water, then dried in an oven at 60°C for 24 h. 0.2 g of desiccated dye is dissolved in 40 ml of isopropyl alcohol and 3 ml of glacial acetic acid, stirred for 10 min at 70°C, and added to 50 µl of HNO$_3$ acid, causing the solution to turn red.

2.2 Preparation of Photoanodes

The experiment involved mixing different concentrations of graphene oxide (0.5, 1, 2, 3, 4, and 5% w/v) with 4% (w/v) TiO$_2$ suspensions. The concentrations are 0.5:4, 1:4, 2:4, 3:4, 4:4, and 5:4% (w/v), respectively. After stirring for 30 min, the mixtures are sonicated for 5 min. The resulting mixtures are sprayed onto a fluorine-doped tin oxide glass (FTO) substrates, conducting (10 Ω cm^{-1}) having an effective area of 1×1 cm^2, heated to 400°C, and then immersed in an anthocyanin dye solution for 12 h as shown in Fig. 1(a).
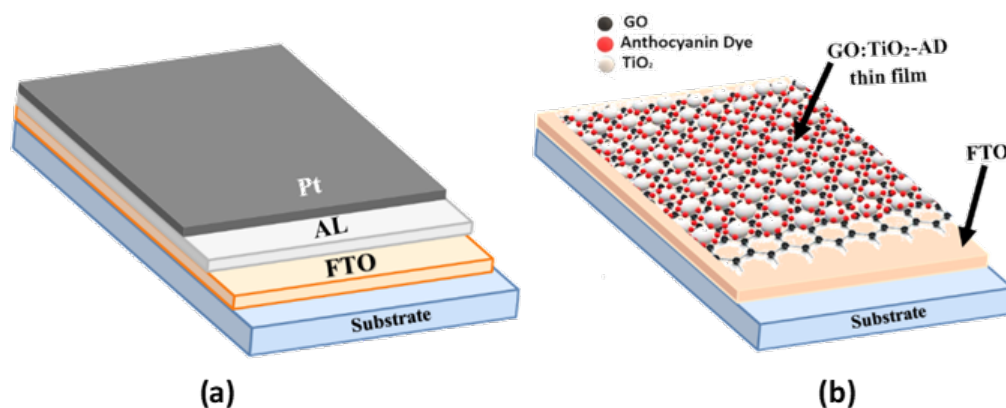
Figure 1 (a) Photoanode electrode and (b) counter electrode for prepared DSSC.

2.3 Preparation of Counter Electrode

Fig. 1(b) exhibit counter electrode. A thin layer (100 nm) of Al is deposited on FTO glass with an area of 1×1 cm^2 via thermal evaporation, and Pt is deposited on the Al layer via decomposition of H_2PtCl_6 by spry pyrolysis technique at 400 °C for 30 min.

2.4 Preparation Electrolyte

0.127g of iodine (I_2) is dissolved in 10 ml of ethylene glycol. Next, 0.83 g of potassium iodide (KI) is added. The solution is stirred and stored in the dark.

2.5 Assembling of DSSC

A sealed sandwich type cell is formed by combining the counter electrode with the photoanode as in Fig. 2(a). A little amount of redox electrolyte is inserted between the two plates, namely the dye-dipped photoanode and the counter electrode. The combination is employed as a redox pair to enhance the properties of the electrolyte and the operational efficacy of DSSCs. The dye sensitized electrode is placed vertically above the counter electrode and fastened together using binder clips as shown in Fig. 2(b).

2.6 Characterization Techniques

The crystal structure of the films is studied using an (Aeris) XRD. The morphology and topography of films are analyzed using (Inspect F50) FESEM, and AFM (Angstrom Advanced Inc., AA2000), respectively. Optical readings are analyzed using a (Shimadzu UV-1900) spectrophotometer.
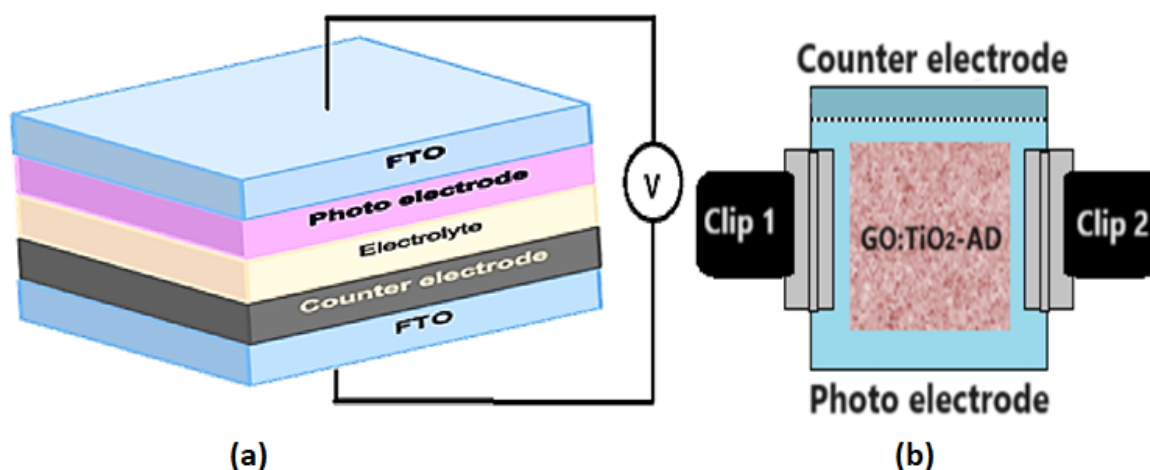
Figure 2 (a) Layers of fabricated DSSC and (b) Schematic of the fabricated DSSC.

The electrical characteristics are analyzed using a Hall Effect measuring device (ECOPIA HMS-3000). The J-V characteristics are measured by computer controlled Keithley 2450 source meter. The measurements are conducted under conventional test conditions with simulated AM 1.5 illumination at an intensity of 100 mW/cm^2.

3. RESULTS AND DISCUSSION
3.1 Structural and Morphological Properties

Fig. 3 shows TiO₂, GO powders, and GO:TiO₂-AD photoanodes with varying GO concentrations deposited on FTO substrates employed in the photoanodes of DSSC. The peak at $2\theta=11.7°$ corresponds to the (001) plan stacked GO sheets with an interlayer spacing of 0.84 nm [21]. The diffraction pattern of TiO₂ and GO:TiO₂-AD photoanodes indicates a maximum intensity peak at $2\theta=25.28°$ corresponds to (101) plane, indicates to the anatase phase [22] for tetragonal structures with a=b=3.77 Å and c=9.49 Å lattice constants, as per JCPDS card number 00-002-0387. Additionally, $2\theta=32.51°$ and $2\theta=50.39°$ have been observed referred to FTO substrates plans (101) and (211) [23].
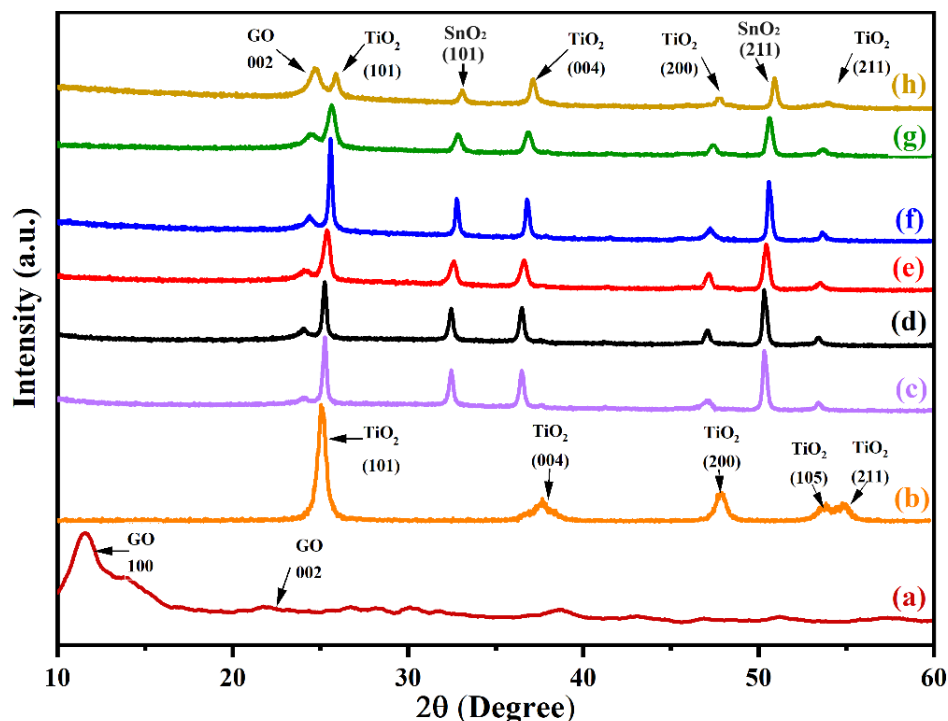
Figure 3 XRD patterns of (a) GO, (b)TiO₂ and (c-h) GO:TiO₂ thin films at concentrations (0.5:4,1:4 , 2:4 , 3:4, 4:4 and 5:4) % respectively.

GO:TiO₂-AD photoanodes have no difference in the diffraction patterns after alteration; just the single diffraction peak of GO disappears at 11.7°, and a distinct peak emerges at 24.21° owing to (002) plane. This indicates that the water included in the substance is removed during synthesis. Inter sheet restacking occurs as a result of Van Der Waals forces. The nanosheet creates a thin conjugate network. Introducing GO into the TiO₂ lattice alters the electronic density at the crystallographic location, leading to significant effects on scattering parameters and XRD peak intensities [24].
The Scherrer formula estimated TiO₂, GO, and GO:TiO₂-AD crystallite size (D) [25].

$$D = \frac{0.94\lambda}{\beta \cos\theta} \tag{1}$$

where β is the peak's full width at half maximum (FWHM) height and λ is the wavelength of X-ray. Looking at the preferred (hkl) plane of GO (001) and (101) for TiO₂ and GO:TiO₂ powders revealed crystallite sizes. For various GO:TiO₂ concentrations (0.5:4, 1:4, 2:4, 3:4, 4:4, and 5:4), it is found 4.46 nm for GO, 15.65 for TiO₂, 19.84, 19.38, 18.52, 17.32, 16.61, and 15.04 nm. Results reveal that higher GO concentrations due to lower crystallite size then increasing surface area and photo detective.

Fig.4 (a-f) reveal FESEM images of GO:TiO$_2$-AD thin films at varies GO concentrations. This figure demonstrates that GO-TiO$_2$-AD photoanodes exhibit a uniform surface morphology characterized by several randomly distributed chunks or aggregates of GO. The results indicates that GO tended to cluster and spread effectively in the GO-TiO$_2$-AD photoanodes. An increase GO concentration is due to formation of a continuous network with TiO$_2$. The network comprises channels that allow charge carriers to flow through, specifically those pathways with low electrical resistance [26,27]. Additionally, studies have demonstrated that adding GO to TiO$_2$ photoelectrode creates a rough and porous surface due to the distinctive two-dimensional structure of GO [28,29].
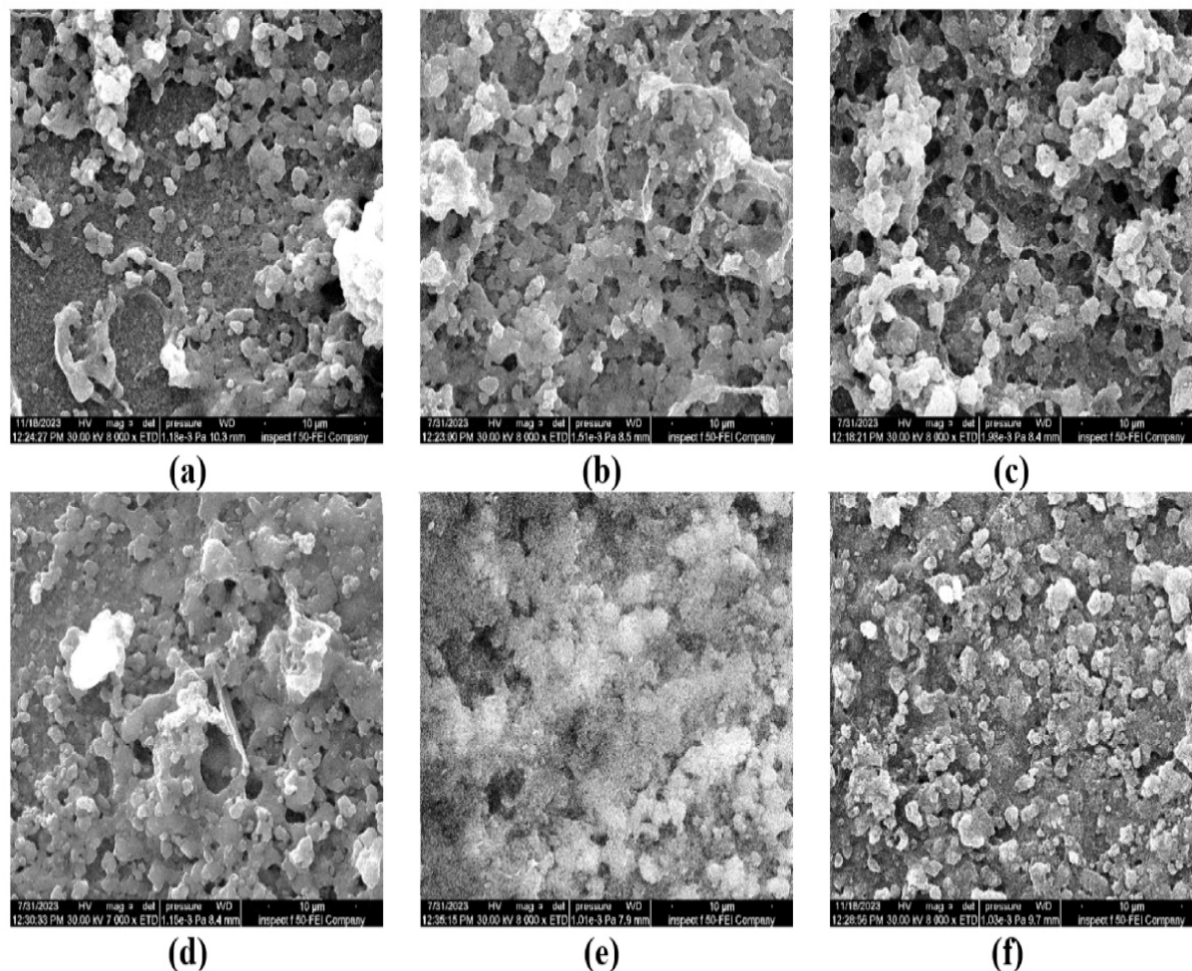
Figure 4 FESEM images of GO:TiO$_2$-AD thin films at varies GO concentrations % (a) 0.5:4 (b) 1:4 (c) 2:4 (d) 3:4 (e) 4:4 (f) 5:4.

Fig.5 (a-f) display AFM analysis for the 2D and 3D surface structures of the GO:TiO$_2$ photoanodes containing 0.5, 1, 2, 3, 4, and 5 wt.% of GO, respectively. Table 1, exhibit the roughness is increased from 16.8 nm for 0.5:4 GO:TiO$_2$-AD to 41.7 nm for 5:4 GO:TiO$_2$-AD and root mean square (RMS) of same concentrations is increased from 19.5 nm to 48 nm. At the same time, the average diameter of grain size decreases from 60.9 to 52.8 nm with increased GO concentrations. The elevated surface roughness (16.8-28.5nm), of the GO: TiO$_2$ thin film suggests a large surface area, leading to enhance dye absorption. During the annealing process at 400 °C, the evaporation of water in GO led to an increase in the porosity of the GO:TiO$_2$ thin film due to volume shrinkage. The porous structure of thin films enhances light scattering, and dye absorption, and improves photovoltaic characteristics [30,31].
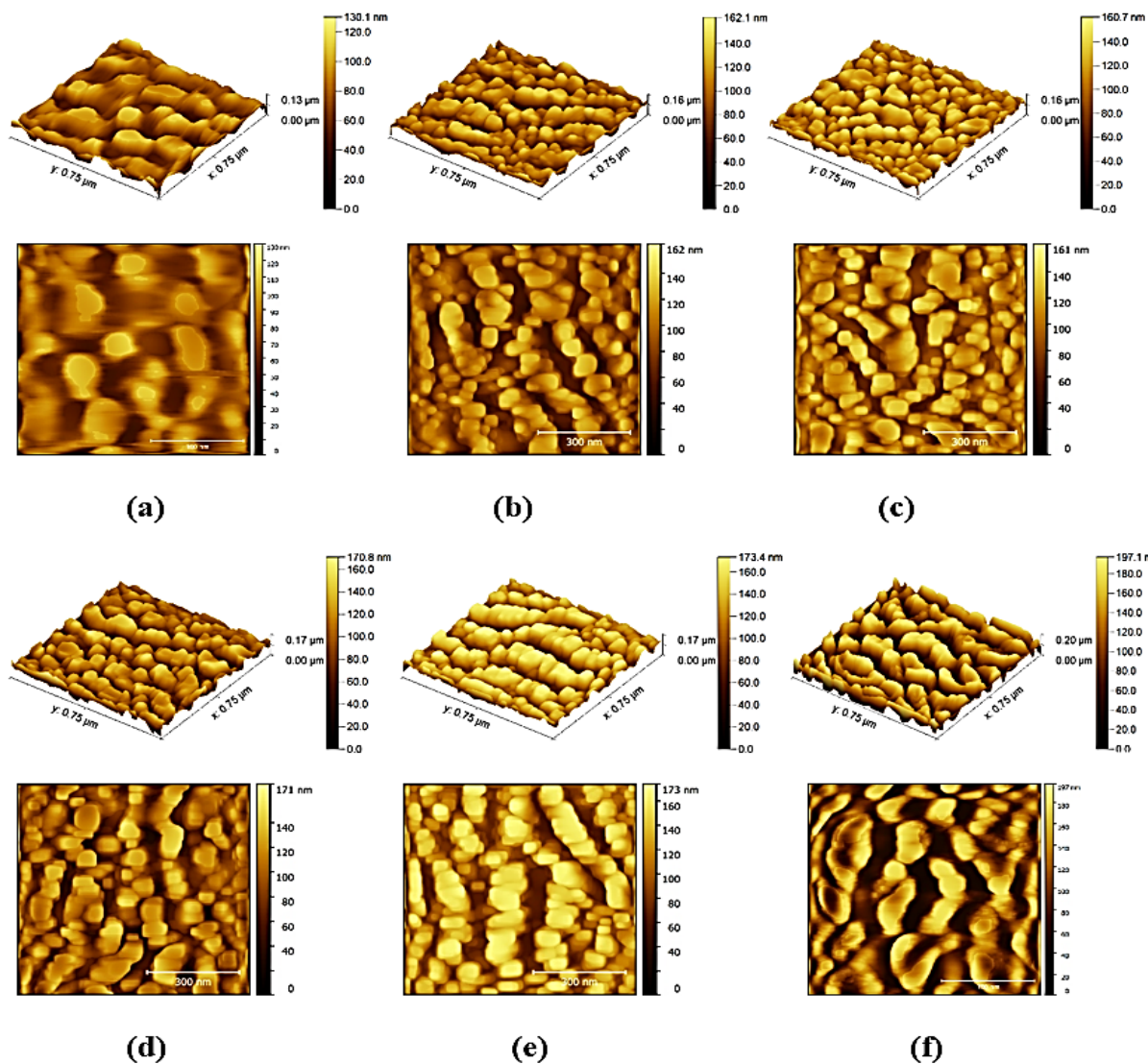
Figure 5 AFM 2D and 3D images of GO:TiO$_2$-AD photoanodes at varies GO concentrations % (a) 0.5:4 (b) 1:4 (c)2:4 (d) 3:4 (e)4:4 (f) 5:4.

Table 1 Morphology parameters for the prepared GO:TiO$_2$-AD with various GO concentrations.

Samples	RMS(nm)	Roughness (nm)	Average Diameter (nm)
0.5:4 GO:TiO$_2$-AD	19.5	16.8	60.9
1:4 GO:TiO$_2$-AD	26.4	22.8	65.3
2:4 GO:TiO$_2$-AD	27.1	23.5	61.8
3:4 GO:TiO$_2$-AD	31.7	27.4	69.6
4:4 GO:TiO$_2$-AD	32.9	28.5	69.3
5:4 GO:TiO$_2$-AD	48	41.7	52.8

3.2 Optical Properties

Fig.6, displays the visible region absorption spectra of the GO:TiO$_2$-AD photoanodes. they exhibit characteristic absorption at around 580 nm and in the 400–800 nm range. As GO is loaded into the

GO:TiO$_2$-AD photoanodes the intensity of the absorption peak rises. Furthermore, increased dye adsorption indicates increased TiO$_2$ film surface area [32]. Chemical adsorption of these dyes onto the surface of TiO$_2$ is commonly acknowledged to result from the condensation of alcoholic bound protons with the hydroxyl functional groups present on the nanocrystalline TiO$_2$ surface [33]. Anthocyanins contain chromophore groups within their chemical composition, enabling them to selective absorb light within the visible range of the electromagnetic spectrum [34,35]. On the other side, the anthocyanin dye molecule's anchoring is facilitated by the carboxyl group to the electron-rich GO, which is present on its surface in large quantities. According to the obtained results, the dye loading has increased about the GO content. Increased dye loading can help the photoanode's ability to absorb sunlight [4]. This demonstrated that the prepared photoanodes had a greater capacity for light absorption and dye adsorption, both are very beneficial in raising the DSSC system's energy conversion efficiency [19].
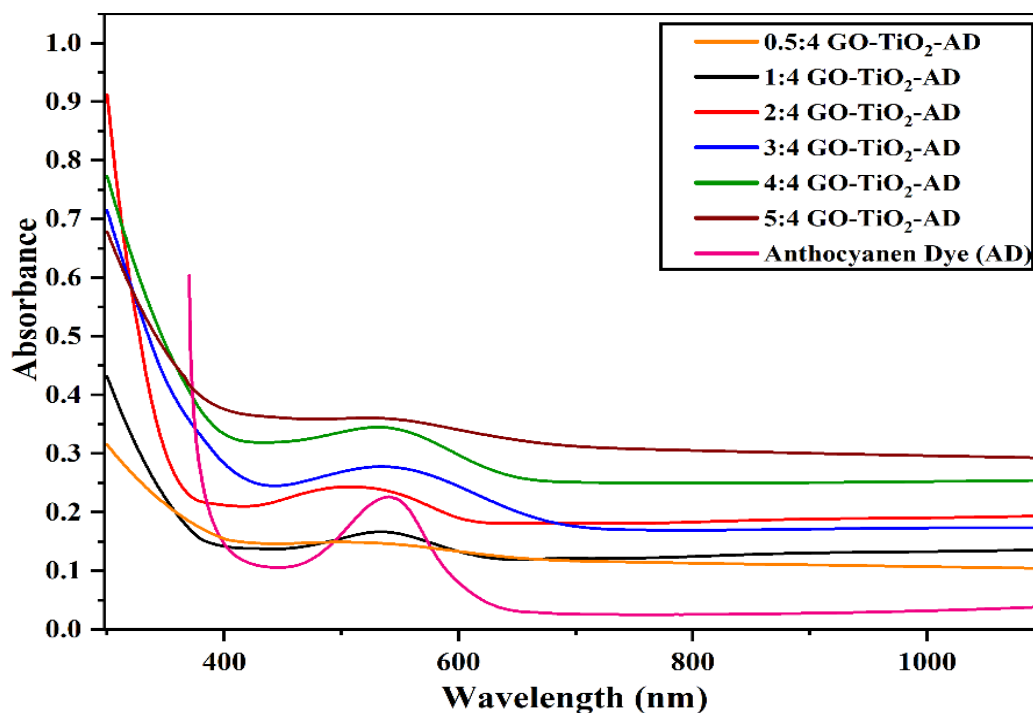
Figure 6 Absorbance spectra of anthocyanin dye and GO:TiO$_2$-AD photoanodes with various GO concentrations.

3.3 Electrical Properties

The electrical characteristics of GO:TiO$_2$-AD thin films are obtained by performing Hall measurements on a glass substrate with an average thickness of 600 nm. Table 2 presents the electrical characteristics at room temperature, including resistivity (ρ), mobility (μ), carrier concentration (n), and conductivity (σ). Research indicates that GO concentration influences the electrical properties of thin films. The conductivity and carrier concentration increase about one and three order of magnitude respectively, whereas the mobility decrease. GO often bears a negative charge due to the presence of oxygen containing functional groups, including carboxyl, hydroxyl, and epoxide groups, on its surface. Anthocyanin dyes are usually negatively charged because of their conjugated double bond systems and many hydroxyl groups, which may delocalize electrons and provide a net negative charge sites will supply two more free electrons, lowering the resistivity of the film. The reduction in the film's resistivity validates a rise in the concentration and conductivity of carriers. This high conductivity is ascribed to GO, which lowers the interfacial resistance between TiO$_2$ nanoparticles [36,37]. The

enhanced electrical conductivity seen in GO:TiO$_2$-AD films is the primary prerequisite for increased DSSC efficiency.

Table 2 Hall Effect parameters of GO:TiO$_2$-AD thin films with various GO concentrations.

Sample	$\sigma_{R.T} \times 10^{-6}$ $(\Omega.cm)^{-1}$	$\rho_{R.T} \times 10^5 (\Omega.cm)$	$\mu \times 10^1$ (cm^2/V. s)	n $\times 10^{11}$ (cm^{-3})
0.5:4 GO:TiO$_2$-AD	2.338	4.277	41.3	3.532
1:4 GO:TiO$_2$-AD	3.185	3.14	22.4	8.849
2:4 GO:TiO$_2$-AD	7.778	1.286	16.8	28.79
3:4 GO:TiO$_2$-AD	3.019	3.312	4.76	39.54
4:4 GO:TiO$_2$-AD	3.731	2.680	1.59	145.7
5:4 GO:TiO$_2$-AD	59.81	16.72	1.39	2672

3.4 J-V Characterizations of DSSC

The J-V characteristics are measured of DSSC under standard test conditions with simulated AM 1.5G illumination at an intensity of 100 mW.cm^{-2}. Fig.7 shows the schematic of mechanism of FTO/GO: TiO$_2$-AD/Active layer/FTO solar cell operate. The photon absorbed by the anthocyanin dye causes an electron to move from the ground state to the excited state of the dye (Dye*). The electrons, once excited, go from C.B of TiO$_2$ to the FTO glass via a graphene oxide sheet. After traveling via an external circuit, the electrons are returned to the dye-sensitized solar cell at the counter electrode. The electrolyte transfers an electron to the dye molecule, creating a positively charged dye ion (Dye$^+$), which helps complete the circuit, as seen in Fig.7(a).
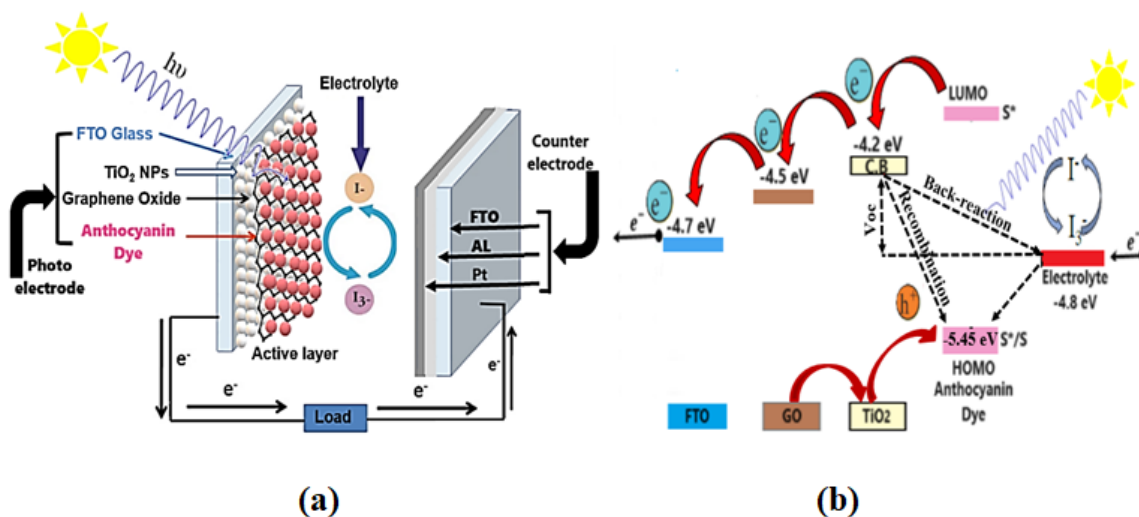
Figure 7 Schematic illustrate the work mechanism for fabricated GO:TiO$_2$-AD DSSC.

The effectiveness of a DSSC is determined by four energy levels, the excited state which is lowest occupied molecular orbital (LUMO) and the ground state, which is highest occupied molecular orbital (HOMO) of the photosensitizer, the Fermi level of the TiO$_2$ electrode, and the redox potential of the mediator (I$^-$/I^{-3}) in the electrolyte [38]. Fig. 7(b) the work function of GO (4.4 eV) is lower than the

conduction band of TiO$_2$ (4.2 eV). Placing GO between TiO$_2$ and FTO allows electrons to go from TiO$_2$ to FTO but prevents electron flow in the other way [39]. Moreover, the work function of GO closely resembles that of FTO (4.7 eV). Therefore, modifying the surface of FTO with GO serves as an extra electron-collecting electrode, which lead to a substantial increase in the charge transport rate within the transparent conducting electrode. This enhancement ultimately improves the performance of the device [40].

Fig. 8 (a) and (b) show the typical (J-V) and (P-V) curves respectively of DSSCs fabricated with different GO concentrations in GO:TiO$_2$-AD photoanodes which measured under AM 1.5G illumination. The fill factor (F.F) is calculated by the following equations:

$$F.F = \frac{V_{max} \times J_{max}}{V_{oc} \times I_{sc}} \times 100\%$$

(2)

where V$_{max}$ is the maximum power voltage, J$_{max}$ is the maximum current density, J$_{sc}$ is the short circuit current density and V$_{oc}$ is voltage open circuit which are determined from the Fig. 8(a) and (b). The power conversion efficiency (PCE) of a solar cell is calculated by dividing the power generated by the cell (P$_{max}$) by the power incident on the representative area of the cell (P$_{in}$)[41]:

$$\eta = \frac{P_{max}}{P_{in}} \times 100\%$$

(3)

The series and shunt resistances, R$_S$ and R$_{sh}$, can be estimated by reciprocal of slope Fig. 8(a) at regions which V$_{oc}$ and I$_{sc}$ equal to zero respectively [43]. The parameters of DSSC such as V$_{oc}$, J$_{sc}$, F.F, η, R$_s$ and R$_{sh}$ are listed in Table 3. The results show the inclusion of GO resulted in a notable enhancement in V$_{oc}$, J$_{sc}$, and F.F due to the reduction of carrier recombination and enhancement of contacts at the interface between the semiconducting layer and the transparent conducting electrode. The PCE increases about 3.5 times when the GO concentration rises from 0.5 to 4%, which due to the rapid charge transport mechanism in the photoanode.
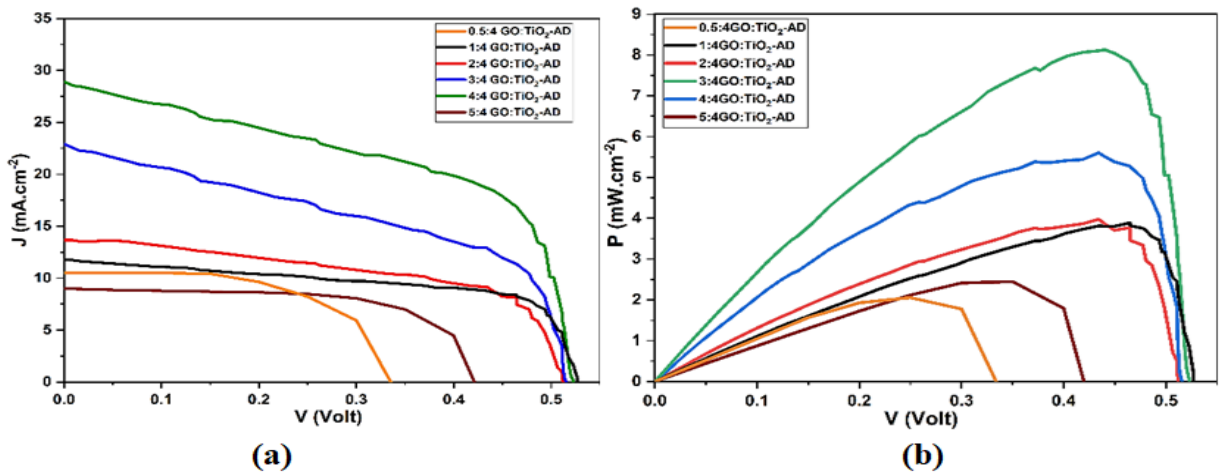
Figure 8 (a) J-V curve and (b) P-V curve of fabricated DSSCs with different GO concentrations under 100 mW/cm^2 illumination.

The concentration of 5% GO exhibited a low power conversion efficiency of 1.52%. This is due to the porous TiO$_2$ layer leaving gaps on the FTO conducting surface, allowing the electrolyte solution to penetrate and cause direct carrier recombination, leading to decreased device performance. Surface modification of the FTO substrate is essential for creating high-performance DSSCs [44-46].

Table 3 Parameters of GO:TiO$_2$-AD DSSCs with various concentrations of GO.

Sample	V_{oc} (V)	J_{sc}(mA/cm^2)	F.F(%)	η(%)	R_S(Ω.cm)	R_{Sh}(Ω.cm)
0.5:4 GO:TiO$_2$-AD	0.41	8.9	65.77	1.82	0.038	4.32
1:4 GO:TiO$_2$-AD	0.52	11.6	60.64	2.80	0.063	0.89
2:4 GO:TiO$_2$-AD	0.51	13.8	55.31	2.95	0.046	1.48
3:4 GO:TiO$_2$-AD	0.51	22.9	46.82	4.17	0.041	0.46
4:4 GO:TiO$_2$-AD	0.52	28.85	53.79	6.14	0.030	0.45
5:4 GO:TiO$_2$-AD	0.33	10.4	58.28	1.52	0.23	3.47

4. CONCLUSIONS

A hybrid GO: TiO$_2$-AD nanocomposites with different GO concentrations have been used as photoanode in fabrication of DSSCs. The various measurements have been confirmed formation of the GO: TiO$_2$ nanocomposite. These changes in GO concentrations ultimately have been enhanced the ability of the photoanodes to absorb dye, harvest light, and generate a higher photocurrent density. The incorporation of GO into the TiO$_2$ results in the enhancement of device parameters J$_{SC}$, V$_{OC}$ and PCE. As the GO concentration increases from 0.5 to 4 wt%, the PCE increases from 1.82 to 6.14 %. GO offers an improved rate of collection and transport of electrons except for 5%. The enhanced electrical conductivity seen in GO: TiO$_2$-AD photoanodes is the primary prerequisite for increased dye sensitized solar cells efficiency.

References

[1] N. Armaroli, V. Balzani, Angew. Chem. 46 (2006) 5
[2] R.D. Costa, D.M. Guldi, Carbon nanomaterials as integrative components in dye-sensitized solar cells, De Gruyter eBooks (2014) 475
[3] Y.-C. Wang, C.-P. Cho, J. Photochem. Photobiol. A Chem. 332 (2017) 1
[4] M. Khannam, S. Sharma, S. Dolui, S.K. Dolui, RSC Adv. 6 (2016) 55406
[5] A.K. Jeryo, Q.A. Abbas, Iraqi J. Sci. 61 (2020) 2241
[6] D. Augustine, E.S. Rosa, N. Prastomo, S. Shobih, J. Elektronika Telekomunikasi 20 (2020) 2
[7] H. Abed, M. Alsultani, M. Abdulsattar, H. Abduljalil, Egypt. J. Chem. 36 (2019) 2009
[8] A. Al-Shawi, M. Alias, P. Sayers, M.F. Mabrook, Micromachines 10 (2019) 643
 [9] P. Gnida, P. Jarka, P. Chulkin, A. Drygała, M. Libera, T. Tański, E. Schab-Balcerzak, Materials 14 (2021) 1633
[10] H.A. Hessain, J.J. Hassan, Iraqi J. Sci. 61 (2020) 1313
[11] A.J.Al-Douri, M.F.A.Alias, M.N.Makadsi, G.H.Mohammed , A.A.Alnajjar, Thin Solid Films, 517 (2008) 881
[12] M.W. Kazem, R.K. Jamal, Iraqi J. Sci. 62 (2021) 1893
[13] T.-F. Yi, S.-Y. Yang, Y. Xie, J. Mater. Chem. A 3 (2015) 5750
[14] G.H. Jetani, M.B. Rahmani, Eur. Phys. J. Plus 135:720 (2020) 1
[15] H. Hug, M. Bader, P. Mair, T. Glatzel, Appl. Energy 115 (2014) 21
[16] W. Routray, V. Orsat, Compr. Rev. Food Sci. Food Saf. 10 (2011) 303
[17] C.-Y. Chien, B.-D. Hsu, Sol. Energy 98 (2013) 203
[18] S. Junling, Y. Zongyou, Y. Zijiang, A. Pitchamuthu, W. Shixin, Y. Jun, Z. Yang, D. Wei-Qiao, Z. Hua, Liu, Xue-Wei, Chem. 17 (2011) 10832
[19] L. Wei, P. Wang, Y. Yang, Z. Zhan, Y. Dong, W. Song, R. Fan, Inorg. Chem. Front. 5 (2018) 54
[20] S.R. Kim, Md. K. Parvez, M. Chhowalla, Chem. Phys. Lett. 483 (2009) 124
[21] S. Prabakaran, K.D. Nisha, S. Harish, J. Archana, M. Navaneethan, S. Ponnusamy, C. Muthamizhchelvan, Y. Hayakawa, Appl. Surf. Sci. 449 (2018) 332

[22] S. Jamil, M. Fasehullah, Mater. Innov. 1 (2021) 22

[23] M.K. Ahmad, N.A. Marzuki, C.F. Soon, N. Nafarizal, R. Sanudin, A.B. Suriani, A. Mohamed, M. Shimomura, K. Murakami, M.H. Mamat, M.F. Malek, AIP Conf. Proc; 2017

[24] S. Manu, M.A. Khadar, J. Mater. Chem. C 3 (2015) 1846

[25] B.D. Cullity, Elements of X-Ray Diffraction, Franklin Classics, 2nd ed; 2018

[26] W. Vallejo, A. Rueda, C. Díaz-Uribe, C. Grande, P. Quintana, R. Soc. Open Sci. 6 (2019) 181824

[27] A. Aprilia, V. Marcelina, F. Yuliasari, Y.W. Hartarti, Fitrilawati, L. Safriani, R.E. Siregar, Mater. Sci. Forum 966 (2019) 378

[28] M.-Y. Yen, M.-C. Hsiao, S.-H. Liao, P.-I. Liu, H.-M. Tsai, C.-C.M. Ma, N.-W. Pu, M.-D. Ger, Carbon 49 (2011) 3597

[29] A.M. Ramli, M.Z. Razali, N.A. Ludin, Malaysian J. Anal. Sci. 21 (2017)

[30] X. Fang, M. Li, K. Guo, Y.Z. Hu, X. Liu, B. Chen, X. Zhao, Electrochim. Acta 65 (2012) 174

[31] H. Wang, S.L. Leonard, Y.H. Hu, Ind. Eng. Chem. Res. 51 (2012) 10613

[32] L. Zhang, Z.-S. Wang, J. Mater. Chem. C 4 (2016) 3614

[33] R. Ramamoorthy, K. Karthika, A. Maggie Dayana, G. Maheswari, V. Eswaramoorthi, N. Pavithra, S. Anandan, R. Victor Williams, J. Mater. Sci. Mater. Electron. 28 (2017) 13678

[34] J. Song, X. Wang, C.T. Chang, J. Nanomater. 2014 (2014) 1

[35] N. Ahmadiani, R.J. Robbins, T.M. Collins, M.M. Giusti, J. Agric. Food Chem. 62 (2014) 7524

[36] H. Wang, L. Nie, J. Li, Y. Wang, G. Wang, J. Wang, Z. Hao, Chin. Sci. Bull. 58 (2013) 724

[37] N. Yang, J. Zhai, D. Wang, Y. Chen, L. Jiang, ACS Nano 4 (2010) 88

[38] H. Khudier, M. Al-Bahrani, J. Coll. Educ. 9 (2019) 227

[39] T. Chen, W. Hu, J. Song, G.H. Guai, C.M. Li, Adv. Funct. Mater. 22 (2012) 5245

[40] A. Okello, B.O. Owuor, J. Namukobe, D. Okello, J. Mwabora, Heliyon 7 (2021) e06571

[41] K. Sharma, V. Sharma, S.S. Sharma, Nanoscale Res. Lett. 13 (2018)

[42] A. Hegazy, N. Kinadjian, B. Sadeghimakki, S. Sivoththaman, N.K. Allam, E. Prouzet, Sol. Energy Mater. Sol. Cells 153 (2016) 108

[43] K. Ramalingam, C. Indulkar, Distrib. Gener. Syst. (2017) 69

[44] M.U. Shahid, N.M. Mohamed, M. Khatani, A.S. Muhsan, A. Samsudin, M.I. Irshad, S.N.A. Zaine, AIP Conf. Proc; 2017

[45] Badis Bendjemil, Maram Mechi, Khaoula Safi, Mounir Ferhi, Karima Horchani Naifer, Exp. Theo. NANOTECHNOLOGY 8 (2024) 51

[46] A. M. Ahmed Alwaise, Raqeeb H. Rajab, Adel A. Mahmood, Mohammed A. Alreshedi, Exp. Theo. NANOTECHNOLOGY 8 (2024) 67